

Relativistic current densities for bound spin–orbit partners and the longitudinal–transverse response in $(e,e'p)$ processes

J.A. Caballero^{1,2}, T.W. Donnelly³, E. Moya de Guerra² and J.M. Udías⁴

¹*Departamento de Física Atómica, Molecular y Nuclear
Universidad de Sevilla, Apdo. 1065, E-41080 Sevilla, SPAIN*

²*Instituto de Estructura de la Materia, Consejo Superior de Investigaciones Científicas
Serrano 123, E-28006 Madrid, SPAIN*

³*Center for Theoretical Physics, Laboratory for Nuclear Science and Dept. of Physics
Massachusetts Institute of Technology, Cambridge, MA 02139, USA*

⁴*Departamento de Física Atómica, Molecular y Nuclear
Universidad Complutense de Madrid, E-28040 Madrid, SPAIN*

Abstract

Scalar, baryon and vector–current densities in coordinate and momentum space are calculated within a relativistic mean–field model. The role of the low components of the bound nucleon wave function is investigated in detail for different spin–orbit partner shells. We show that the relative importance of the negative–energy projection components can be explained from the different quantum numbers involved in the relativistic wave function. This fact has proved to be important in the analysis of various electron scattering observables even for low–medium values of the bound nucleon momentum.

PACS: 25.30.Fj; 24.10.Jv; 21.10.Jx

Keywords: Quasielastic electron scattering; Spin–orbit partners; Negative energy projections; Scalar, baryonic and vector current densities; Longitudinal–transverse response function.

1. Introduction

In a recent publication [1] we investigated the role of the negative-energy projections (NEP) of the relativistic bound nucleon wave function in the longitudinal (L), transverse (T, TT) and longitudinal-transverse (TL) response functions of $(e, e'p)$ processes. Our work was motivated by the success in the interpretation of recent $(e, e'p)$ data [2] of the relativistic distorted wave impulse approximation (RDWIA) [3, 4, 5] that uses relativistic bound and scattering wave functions (based on the S-V Walecka model [6, 7] and Dirac phenomenology). Data on momentum distributions obtained from exclusive quasielastic experiments over extended ranges of missing momenta at low missing energies have been successfully analyzed in RDWIA producing reasonable values of the spectroscopic factors ($s_\alpha \sim 0.7$ for the $s_{1/2}$ shell in ^{208}Pb) consistent at low and high momentum [3, 8].

The study carried out in ref. [1] was made in the relativistic plane wave impulse approximation (RPWIA) that differs from RDWIA in that the scattered nucleon is described as a plane wave. Both RPWIA and RDWIA calculations can also be found in refs. [9, 10, 11]. The present work focusses on the TL response in RPWIA for the reasons discussed below.

The investigation in ref. [1] was focused on the relativistic plane-wave impulse approximation (RPWIA) with the purpose of isolating effects due to the relativistic bound nucleon wave function and current. We discussed the results for three choices of the nucleon current gauge: Landau or NCCi, Coulomb or CCI(0) and Weyl or CCI(3). We also considered two current operators that are called $i=1,2$ following de Forest's notation [12]. It was found that the role of the NEP of the relativistic bound nucleon wave function in RPWIA is to cause a reduction of the differential cross section at low p ($p \leq 300$ MeV) and an increase at high p ($p \geq 300$ MeV). In RPWIA [1], the reduction at low p is generally small and depends little on the current operator and gauge choice with one proviso: the Weyl gauge choice may produce up to 20% deviations from Landau and Coulomb gauges at low p . However this deviation is also present when the NEP of the relativistic bound nucleon wave functions is neglected. It is known to be due to the difference between $\sigma_{CC(0)}$ and $\sigma_{CC(3)}$ defined in ref. [12], therefore appearing even when non-relativistic (n.r.) bound nucleon wave functions are used [13]. At larger p values ($p \geq 300$ MeV) the size of the NEP contributions depends largely on the choice of the current operator and gauge. The NEP contributions are minimized for the Landau and Coulomb gauge and for $i=2$ current operator, while the Weyl gauge and the $i=1$ current operator tend to maximize the effect of the NEP contributions, producing large differences in some of the response functions. This is particularly the case for the TL response function (R^{TL}) where we found variations of up to a factor of three.

At present a certain degree of controversy surrounds the TL responses obtained from exclusive quasielastic electron scattering experiments for the least bound orbitals in several nuclei (^{12}C , ^{16}O , ^{208}Pb): in some cases [14] large deviations from standard DWIA calculations appear while in others [15] the data are close to the DWIA calculations.

Since our study in ref. [1] was focused on the $p_{1/2}$ shell in ^{16}O , it is interesting to know to what extent the above mentioned discrepancy by a factor three remains when knockout from other orbitals is considered. Hence in the present work we extend our study to the $1p_{3/2}$ orbital (in ^{12}C and ^{16}O), as well as to the $1d_{3/2}$, $1d_{5/2}$ orbitals in ^{40}Ca . The aim here is to see whether the large effect on the R^{TL} response found in ref. [1] is a general feature present in other shells, or is particular to the $1p_{1/2}$ shell considered in our recent studies.

With this goal in mind we restrict ourselves to the RPWIA, as in our previous work. Of course, before detailed comparisons can be made with experimental data it is necessary to incorporate the effects of final-state interactions (FSI) in a full RDWIA approach. Although FSI are needed for a quantitative comparison with experimental data [3, 4, 8], we expect that, at least for the largest contributions to the cross section (i.e., excluding from this statement some of the smaller responses, especially some of those that involve polarization degrees of freedom), the effects of FSI to be basically the same for one-nucleon knockout from different bound orbitals, provided the outgoing kinetic energy is the same. At the maximum of the TL response that forms the focus of the present work one finds that for instance for the $p_{1/2}$ and $p_{3/2}$ shells in ^{16}O the FSI effects differ at most by a 4% [16]. We therefore expect that the conclusions of our study here can be extrapolated to the more realistic situation when RDWIA

calculations are performed. On the other hand the present study is necessary to identify the dependence on the NEP of the bound nucleon wave function for different orbitals.

The organization of this paper is as follows: in Section 2 we introduce, within the context of the Walecka model, the scalar, baryonic and vector densities in coordinate and momentum space. Results for various spin-orbit partners are shown and discussed. In Section 3 we study the transverse-longitudinal response function for one-nucleon knockout from a selection of relativistic bound orbitals. We compare and discuss the results obtained for different current operators and gauges and the role of the negative energy projections of the relativistic bound nucleon wave function is studied. Finally in Section 4 we present a summary and our conclusions.

2. Bound nucleon wave functions and densities of spin-orbit partners

As is well known, in the Walecka model [6, 7] the Dirac equations for bound nucleons in a finite nucleus are derived from an interacting relativistic field theory of mesons and baryons by approximating the meson field operators by classical fields. For spherically symmetric spin and isospin saturated nuclei treated within the context of the Hartree approximation only scalar, $S = S(r)$, and vector, $V_\mu = (V(r), \mathbf{0})$, potentials are to be considered and we write the time-independent Dirac equation with $S - V$ potentials as

$$\left[\gamma_0 \tilde{E} - \boldsymbol{\gamma} \cdot \mathbf{p} - \tilde{M} \right] \psi = 0 \ , \quad (1)$$

with

$$\tilde{M} = M - S \ , \quad (2)$$

$$\tilde{E} = E - V \ , \quad (3)$$

where M is the nucleon mass and E is the total energy eigenvalue (that is, $e \equiv M - E > 0$ for bound states). Here and in what follows the conventions of Bjorken and Drell [17] are followed. From eq. (1) two Schrödinger-like equations can be derived for the upper and lower bispinor components of ψ :

$$\psi^\kappa = \begin{pmatrix} \psi_{up}^\kappa \\ \psi_{down}^\kappa \end{pmatrix} \ , \quad (4)$$

$$\left[\nabla^2 + \frac{1}{A_+} \frac{\partial A_+}{\partial r} \left(\frac{\boldsymbol{\sigma} \cdot \boldsymbol{\ell}}{r} - \frac{\partial}{\partial r} \right) + A_+ A_- \right] \psi_{up}^\kappa(\mathbf{r}) = 0 \ , \quad (5)$$

$$\left[\nabla^2 + \frac{1}{A_-} \frac{\partial A_-}{\partial r} \left(\frac{\boldsymbol{\sigma} \cdot \boldsymbol{\ell}}{r} - \frac{\partial}{\partial r} \right) + A_+ A_- \right] \psi_{down}^\kappa(\mathbf{r}) = 0 \ , \quad (6)$$

with

$$A_\pm \equiv \tilde{E} \pm \tilde{M} \ , \quad (7)$$

$$A_+ A_- = \tilde{E}^2 - \tilde{M}^2 = \tilde{K}^2 \ . \quad (8)$$

or

$$\tilde{K}^2 = K^2 + 2MU_{central} \quad (9)$$

with

$$K^2 = E^2 - M^2 \quad (10)$$

and

$$U_{central} = \frac{V^2 - S^2 - 2EV + 2MS}{2M} \quad (11)$$

Here we have defined $K^2 = E^2 - M^2 < 0$ for bound states, and a central potential $U_{central}$ that depends on the energy E . Eqs.(5) and (6) are Schrödinger-like equations for the upper and lower components, respectively, containing in addition to the kinetic energy and central potential ($U_{central}$) terms, a spin-orbit ($\frac{1}{A_{\pm}} \frac{\partial A_{\pm}}{\partial r} \frac{\boldsymbol{\sigma} \cdot \boldsymbol{\ell}}{r}$) term and a Darwin ($\frac{1}{A_{\pm}} \frac{\partial A_{\pm}}{\partial r} \frac{\partial}{\partial r}$) term. The last two being generally different for the upper and lower components.

We recall that in the relativistic case the bound nucleon wave function is labeled by the quantum number κ that characterizes the eigenvalues of total angular momentum and parity of the four-spinor. The relativistic parity operator $\Pi = \gamma^0 P$, with $P\phi(\mathbf{r}) = \phi(-\mathbf{r})$, has the eigenvalue $\Pi = (-1)^{\kappa} \frac{\kappa}{|\kappa|}$ and the j -eigenvalue is $j = |\kappa| - \frac{1}{2}$. In standard notation ψ^{κ} is written as

$$\psi_m^{\kappa}(\mathbf{r}) = \begin{pmatrix} g_{\kappa}(r)\phi_m^{\kappa}(\hat{r}) \\ i f_{\kappa}(r)\phi_m^{-\kappa}(\hat{r}) \end{pmatrix}, \quad (12)$$

with

$$\phi_m^{\kappa} = \sum_{\Lambda\sigma} \langle \ell\Lambda \frac{1}{2}\sigma | jm \rangle Y_{\Lambda}^{\ell} \chi_{\sigma}, \quad (13)$$

$$\phi_m^{-\kappa} = -\boldsymbol{\sigma} \cdot \hat{\mathbf{r}} \phi_m^{\kappa} = \sum_{\Lambda\sigma} \langle \bar{\ell}\Lambda \frac{1}{2}\sigma | jm \rangle Y_{\Lambda}^{\bar{\ell}} \chi_{\sigma}. \quad (14)$$

The relationship between κ , j , ℓ and $\bar{\ell}$ is:

For $\kappa > 0$:

$$\kappa = j + \frac{1}{2} = \ell = \bar{\ell} + 1, \quad \Pi = (-1)^{\ell}. \quad (15)$$

For $\kappa < 0$:

$$\kappa = -\left(j + \frac{1}{2}\right) = -(\ell + 1) = -\bar{\ell}, \quad \Pi = (-1)^{\ell}. \quad (16)$$

Because in studies of nuclear structure we are more familiar with the non-relativistic labeling of single-particle states, in practice it is convenient to resort to the ℓ_j characterization of the wave functions as in the non-relativistic limit, where ℓ is a good quantum number and the spin-orbit partners are the $j = \ell \pm \frac{1}{2}$ states. To fix ideas and to avoid confusion, in what follows we refer to the “stretched” ($j = \ell + \frac{1}{2}$) and “jack-knifed” ($j = \ell - \frac{1}{2}$) partners as the states with $\kappa = -(\ell + 1) < 0$, and $\kappa = \ell > 0$, respectively, with ℓ characterizing the orbital angular momentum of the upper component as in eqs. (12–16). Hence the lower components of the spin-orbit partners have $\bar{\ell} = \ell + 1$ and $\bar{\ell} = \ell - 1$ for the stretched and jack-knifed ℓ_j partners, respectively.

The general formulas above may be cast in various forms — here we write them as equations for upper and lower components with effective central and spin-orbit potentials to bring out the essential differences to be found for the radial wave functions that result. Alternative schemes may be used (for instance, through the introduction of an effective mass; see, for example, [7]), although the present one is sufficient for our purposes. The Schrödinger-like equations for the upper components of the spin-orbit partners are:

For the stretched case ($j = \ell + 1/2$),

$$\left[\frac{1}{r} \frac{\partial^2}{\partial r^2} r - \frac{\ell(\ell+1)}{r^2} + 2MU_{central} - \frac{1}{A_+} \frac{\partial A_+}{\partial r} \left(\frac{\partial}{\partial r} - \frac{\ell}{r} \right) \right] g_{\kappa} = -K^2 g_{\kappa}(r), \quad (17)$$

For the jack-knifed case ($j = \ell - 1/2$),

$$\left[\frac{1}{r} \frac{\partial^2}{\partial r^2} r - \frac{\ell(\ell+1)}{r^2} + 2MU_{central} - \frac{1}{A_+} \frac{\partial A_+}{\partial r} \left(\frac{\partial}{\partial r} + \frac{\ell+1}{r} \right) \right] g_{\kappa} = -K^2 g_{\kappa}(r), \quad (18)$$

Here, in close analogy with the usual non-relativistic limit, the equations for the spin-orbit partners differ only in their spin-orbit coupling terms, and these are relatively small.

On the other hand the Schrödinger-like equation for the lower component

$$\left[\frac{1}{r} \frac{\partial^2}{\partial r^2} r - \frac{\bar{\ell}(\bar{\ell}+1)}{r^2} + 2MU_{central} - \frac{1}{A_-} \frac{\partial A_-}{\partial r} \left(\frac{\partial}{\partial r} - \frac{j(j+1) - \bar{\ell}(\bar{\ell}+1) - \frac{3}{4}}{r} \right) \right] f_\kappa = -K^2 f_\kappa , \quad (19)$$

when applied to the spin-orbit partners reads:

For the stretched case ($j = \ell + 1/2$),

$$\left[\frac{1}{r} \frac{\partial^2}{\partial r^2} r - \frac{(\ell+1)(\ell+2)}{r^2} + 2MU_{central} - \frac{1}{A_-} \frac{\partial A_-}{\partial r} \left(\frac{\partial}{\partial r} + \frac{\ell+2}{r} \right) \right] f_\kappa = -K^2 f_\kappa , \quad (20)$$

for the jack-knifed case ($j = \ell - 1/2$)

$$\left[\frac{1}{r} \frac{\partial^2}{\partial r^2} r - \frac{\ell(\ell-1)}{r^2} + 2MU_{central} - \frac{1}{A_-} \frac{\partial A_-}{\partial r} \left(\frac{\partial}{\partial r} - \frac{\ell-1}{r} \right) \right] f_\kappa = -K^2 f_\kappa , \quad (21)$$

Hence, in contrast to the case of the upper components, the equations for the lower components differ not only in the spin-orbit coupling term but also in the centrifugal barrier. This produces stronger differences on the radial dependence of the lower components than on the radial dependence of the upper components. This is to say, if one compares for instance the radial functions f_κ for the $p_{1/2}$ and $p_{3/2}$ cases one expects to see larger differences than if one compares the g_κ for those same shells.

Later we shall see the consequences of these differences in upper and lower components when examining the RPWIA results in detail; here it should be noted that in general the lower components are small and the radial dependence of both scalar and baryonic densities is mostly dominated by the upper components:

$$\rho_S(r) = \frac{4\pi}{2j+1} \sum_m \bar{\psi}_m^\kappa \psi_m^\kappa = [g_\kappa^2(r) - f_\kappa^2(r)] , \quad (22)$$

$$\rho_B(r) = \frac{4\pi}{2j+1} \sum_m \psi_m^{\kappa+} \psi_m^\kappa = [g_\kappa^2(r) + f_\kappa^2(r)] , \quad (23)$$

with

$$\int \rho_B(r) r^2 dr = 1 . \quad (24)$$

In the cases considered here the contribution of f_κ to the normalization is less than 3%. Nevertheless it is important to realize that for spin-orbit partners the lower components can differ significantly, while the differences in the upper components tend to be mild. This is illustrated in fig. 1 where we plot the sum and difference of baryonic and scalar densities (in fm^{-3}) for the spin-orbit partners $p_{1/2}$, $p_{3/2}$ in ^{16}O and $d_{3/2}$, $d_{5/2}$ in ^{40}Ca . The $3s_{1/2}$ orbital in ^{208}Pb is also plotted for comparison. The present calculations follow similar lines to those of ref. [1]; in particular we use the parameters of ref. [18] and the TIMORA code [19]. Clearly the differences of f_κ due to the different centrifugal barriers are maximal in the $p_{1/2}$ - $p_{3/2}$ spin-orbit partners because the lower component for the $p_{1/2}$ partner is an s-wave while for the $p_{3/2}$ is a d-wave. The $d_{3/2}$ - $d_{5/2}$ spin-orbit partners have correspondingly a p-wave and an f-wave as lower components. It is also interesting to see that for the $3s_{1/2}$ case the lower component looks negligibly small and may be expected to play a minor role.

We note that the elementary three-vector current density

$$\mathbf{v} = \bar{\psi}^\kappa \boldsymbol{\gamma} \psi^\kappa \equiv v(r) \hat{\mathbf{v}} \quad (25)$$

is proportional to the product of g_κ and f_κ

$$v(r) = 2g_\kappa(r) f_\kappa(r) . \quad (26)$$

This quantity is also plotted in fig. 2 for the same orbitals shown in fig. 1.

The larger differences seen for the lower components reflect a genuine relativistic effect that cannot be accounted for when non-relativistic bound nucleon wave functions are used. This naturally motivates an

investigation as to whether or not this relativistic effect has observable consequences. Electron scattering at intermediate energies, involving large momentum transfers, is the ideal place to look for such relativistic effects.

In elastic electron scattering one is sensitive to the Fourier transforms of $\rho_B(\mathbf{r})$ and of $\mathbf{v}(\mathbf{r})$ and relativistic calculations have been presented for a few elastic magnetic form factors [20]. A thorough discussion of relativistic calculations of transverse form factors for elastic electron scattering could provide the motivation for future work — however, following our recent studies [1] the focus of this paper is instead placed on the longitudinal–transverse response functions (R^{TL}) for exclusive quasielastic electron scattering (e,e'p). This particular response function depends on linear combinations of scalar, baryonic and vector densities in momentum space

$$\rho_S(p) = \frac{4\pi}{2j+1} \sum_m \bar{\psi}_m^\kappa(\mathbf{p}) \psi_m^\kappa(\mathbf{p}) = g_\kappa^2(p) - f_\kappa^2(p) , \quad (27)$$

$$\rho_B(p) = \frac{4\pi}{2j+1} \sum_m \psi_m^{\kappa+}(\mathbf{p}) \psi_m^\kappa(\mathbf{p}) = g_\kappa^2(p) + f_\kappa^2(p) , \quad (28)$$

$$v(p) = \frac{4\pi}{2j+1} \sum_m \bar{\psi}_m^\kappa(\mathbf{p}) \hat{\mathbf{p}} \cdot \boldsymbol{\gamma} \psi_m^\kappa(\mathbf{p}) = 2 \frac{\kappa}{|\kappa|} g_\kappa(p) f_\kappa(p) , \quad (29)$$

with $\psi_m^\kappa(\mathbf{p})$ the Fourier transform of $\psi_m^\kappa(\mathbf{r})$. The radial functions in momentum space are given by (see, for instance, [1])

$$g_\kappa(p) = \sqrt{\frac{2}{\pi}} \int_0^\infty r^2 dr g_\kappa(r) j_\ell(pr) , \quad (30)$$

$$f_\kappa(p) = \sqrt{\frac{2}{\pi}} \int_0^\infty r^2 dr f_\kappa(r) j_{\bar{\ell}}(pr) . \quad (31)$$

Specifically, the relevant quantities in p-space that enter directly in the calculations of response functions for (e,e'p) processes are the amplitudes $\tilde{\alpha}_\kappa$ and $\tilde{\beta}_\kappa$ of the positive and negative energy projections of the bound nucleon wave function in the expansion:

$$\psi_m^\kappa(\mathbf{p}) = \sum_s \left[\tilde{\alpha}_\kappa(p) u(p, s) \langle s | i^\ell \phi_m^\kappa(\hat{\mathbf{p}}) \rangle + \tilde{\beta}_\kappa(p) v(p, s) \langle s | i^\ell \phi_m^{-\kappa}(\hat{\mathbf{p}}) \rangle \right] , \quad (32)$$

with

$$\tilde{\alpha}_\kappa(p) = \sqrt{\frac{\bar{E} + M}{2M}} \left(g_\kappa(p) - \frac{\kappa}{|\kappa|} f_\kappa(p) \frac{p}{\bar{E} + M} \right) , \quad (33)$$

$$\tilde{\beta}_\kappa(p) = \sqrt{\frac{\bar{E} + M}{2M}} \left(\frac{p}{\bar{E} + M} g_\kappa(p) - \frac{\kappa}{|\kappa|} f_\kappa(p) \right) , \quad (34)$$

where $u(p, s)$ and $v(p, s)$ are the positive and negative energy solutions of the free Dirac equation with $\bar{E} = \sqrt{M^2 + p^2}$. The absolute values of the positive and negative energy projection amplitudes (in fm³) are plotted in fig. 3 for the spin–orbit partners $p_{1/2}$ – $p_{3/2}$ and $d_{3/2}$ – $d_{5/2}$. Note the different scales of the positive and negative energy projections. Note also that in the limit of free nucleons $\tilde{\beta}_\kappa(p) = 0$, and therefore $|\tilde{\beta}_\kappa|^2$ measures the dynamical enhancement of the lower components.

A much larger dynamical enhancement is observed in fig. 3 for the jack-knifed states than for the stretched states. This was expected from our previous discussion on the Schrödinger–like equations for the upper and lower components. As a matter of fact, much can be learnt by looking at the Schrödinger–like equations that follow from the Dirac eq. (1). For instance, as first pointed out by Ginocchio [21] the Schrödinger–like equation for the lower component is the same for relativistic states having the same $\bar{\ell}$ -value but ℓ -values differing by two units (as for instance the $s_{1/2}$ – $d_{3/2}$ or $p_{3/2}$ – $f_{5/2}$,... pairs) when the spin–orbit coupling term in eq. (19) is negligible. This has been identified as the origin of pseudospin symmetry in nuclear spectra by Ginocchio [21]. Another interesting limiting case can be that of quasidegeneracy of levels with equal j and opposite parity that is also present in nuclear spectra [22].

3. Longitudinal–transverse response function

In this section we compare results on the R^{TL} response functions for one–nucleon knockout from various relativistic bound orbitals. The details of the calculations are as in ref. [1] and we do not repeat them here; we use what was called kinematics I in that work, namely quasielastic conditions with $q = 500$ MeV/c and $\omega = 131.56$ MeV. We recall that, using projection techniques, the R^{TL} response can be separated into a contribution from the positive energy projection (R_P^{TL}), a contribution from the negative energy projection (R_N^{TL}), and a crossed term (R_C^{TL}):

$$R^{TL} = R_P^{TL} + R_N^{TL} + R_C^{TL} \quad , \quad (35)$$

with

$$R_P^{TL} = \mathcal{R}_{uu}^{TL} N_{uu}(p) \quad , \quad (36)$$

$$R_N^{TL} = \mathcal{R}_{vv}^{TL} N_{vv}(p) \quad , \quad (37)$$

$$R_C^{TL} = \mathcal{R}_{uv}^{TL} N_{uv}(p) \quad . \quad (38)$$

In eqs. (36–38) the dependence on the nuclear structure is factorized. This dependence is contained in the bound nucleon momentum distributions

$$N_{uu}(p) = (\tilde{\alpha}_\kappa(p))^2 / 4\pi \quad , \quad (39)$$

$$N_{vv}(p) = (\tilde{\beta}_\kappa(p))^2 / 4\pi \quad , \quad (40)$$

$$N_{uv}(p) = -2\tilde{\alpha}_\kappa(p)\tilde{\beta}_\kappa(p)/4\pi \quad . \quad (41)$$

In contrast, \mathcal{R}_{uu}^{TL} , \mathcal{R}_{vv}^{TL} and \mathcal{R}_{uv}^{TL} depend only on the current operator and gauge and are independent of the nuclear structure.

When the nuclear structure is treated in the non–relativistic limit the nucleon current operator is expanded in the basis of positive energy free Dirac spinors (see for instance ref. [23]) and the single–nucleon response function is

$$\mathcal{R}^{TL} = \mathcal{R}_{uu}^{TL} \quad , \quad (42)$$

corresponding to electron scattering from a free (relativistic) nucleon, and

$$R^{TL} \xrightarrow{n.r.} R_P^{TL} \quad . \quad (43)$$

With relativistic bound nucleon wave functions one has additional single–nucleon responses \mathcal{R}_{uv}^{TL} and \mathcal{R}_{vv}^{TL} that do not appear in the scattering of electrons from free nucleons (or antinucleons). The appearance of these terms is due to the nonzero overlap of the bound nucleon wave function with the Dirac sea that results in finite values of the $N_{uv}(p)$ and $N_{vv}(p)$ functions.

In ref. [1] we showed that the single–nucleon responses \mathcal{R}_{uv}^{TL} and \mathcal{R}_{vv}^{TL} change much more with the changes of the current operator and gauges than does the \mathcal{R}_{uu}^{TL} response. Whereas the single–nucleon response \mathcal{R}_{uu}^{TL} has often been studied [24], the \mathcal{R}_{uv}^{TL} and \mathcal{R}_{vv}^{TL} were for the first time identified and studied in ref. [1]. The fact that these responses are more strongly dependent on the choice of the current operator and gauge, results in a larger theoretical ambiguity in the calculated total response R^{TL} when using relativistic bound nucleon wave functions.

As we showed in the previous section, the overlap with the Dirac sea of the bound nucleon wave function depends strongly on the particular ℓ_j orbital under study. Therefore a different sensitivity of the R^{TL} response to the contributions from the negative energy projections can be expected for different orbitals. In particular we show in figs. 4 and 5 that this sensitivity is quite different for the spin–orbit partners $p_{1/2}$ and $p_{3/2}$ or $d_{3/2}$ and $d_{5/2}$.

The longitudinal transverse response functions for one–nucleon knockout from the $p_{1/2}$ and $p_{3/2}$ orbitals in ^{16}O are shown in the top and bottom panels of fig. 4. For each shell results corresponding to the CC1 current operator and to the three different gauges (Landau, Coulomb and Weyl) are shown

on the left panels, while the right hand panels contain the corresponding results for the CC2 current operator.

In these figures one can see that for fixed current operator and shell the Landau and Coulomb gauges give practically the same results, while the Weyl gauge tends to produce important deviations. The importance of these deviations is much higher for the $p_{1/2}$ than for the $p_{3/2}$ shell. This is also the case when changing the current operator. The following ratios are found between the maximum values of the R^{TL} response of the $p_{1/2}$ shell: if we fix the gauge to be the Coulomb gauge, the ratio between the results for the CC1 and CC2 current operators is

$$\frac{R^{TL}(CC1(0))}{R^{TL}(CC2(0))} \simeq 1.5 \quad , \quad (44)$$

and the ratio is larger in the Weyl gauge

$$\frac{R^{TL}(CC1(3))}{R^{TL}(CC2(3))} \simeq 2 \quad . \quad (45)$$

Similar ratios are found when we fix the current operator and compare the results of different gauges

$$\frac{R^{TL}(CC2(3))}{R^{TL}(CC2(0))} \simeq 1.5 \quad , \quad \frac{R^{TL}(CC1(3))}{R^{TL}(CC1(0))} \simeq 2 \quad , \quad (46)$$

leading to the large difference, by as much as a factor of 3, between the CC1(3) and the CC2(0) results, already mentioned in ref. [1].

On the contrary, for the spin-orbit partner $p_{3/2}$ the results between different choices are not that large so the above ratios reach at most a value of 1.2 (that between CC1(3) and CC2(0) results) and in most cases are less than a 10%. In particular for the $p_{3/2}$ case the dependence on the gauge is almost not visible with the CC2 current operator.

We note that R^{TL} contains the product of transverse and longitudinal currents. The transverse current changes only with the current operator (i.e., CC1 or CC2) but it is independent on the gauge. Therefore, for the cases considered, the strong gauge dependence for the $p_{1/2}$ case must come from the longitudinal current. A similar comparison is made in fig. 5 for the $d_{3/2}$ and $d_{5/2}$ spin-orbit partners. It is also the case that the dependence on the current operator and gauge is more pronounced for the jack-knifed than for the stretched cases.

As seen in figs. 6 and 7 when we consider only the contribution from the positive energy projection (i.e., the truncation in eq. (43)) the sensitivity of the R^{TL} response to the choice of the current operator and gauge is similar for the spin-orbit partners $p_{1/2}$ - $p_{3/2}$ and $d_{3/2}$ - $d_{5/2}$. The larger sensitivity obtained for the $p_{1/2}$ and $d_{3/2}$ partners is due to their larger negative energy projections at low p ($p \leq 200$ MeV) that carries larger deviations particularly in the R_C^{TL} term. This is in turn an effect of the Schrödinger-like equations for the lower components of the spin-orbit partners.

4. Final remarks

The main conclusion of this work is that the large deviation [1] in R^{TL} predictions produced by different current operators and gauges takes place for the jack-knifed states ($p_{1/2}$, $d_{3/2}$, ...), but not for the stretched states ($p_{3/2}$, $d_{5/2}$, ...). This genuine relativistic effect stems from the dynamical enhancement of the lower components, and can be traced back to the Schrödinger-like equations for the upper and lower components of the relativistic bound nucleon wave function.

We have shown that this effect can be understood from the quite different behaviour of the dynamical enhancement function $\tilde{\beta}_\kappa$ of the stretched and jack-knifed states. Indeed, from eq. (34) and fig. 3 one can see that from the jack-knifed states (i.e. $p_{1/2}$, $d_{3/2}$, ...) the amplitudes of the negative energy projections are much larger than those for the stretched states ($p_{3/2}$, $d_{5/2}$, ...). One has to realize that in eq. (34)

$\tilde{\beta}_\kappa(p)$ goes like the difference of two functions of p with the same number of nodes ($n + \ell + 1$) for the stretched states, while for the jack-knifed ones, it goes like the difference of a function with $n + \ell + 1$ nodes and a function with $n + \ell - 1$ nodes ($n = 1$ in the cases considered here). This is due to the different quantum number $\bar{\ell}$ of the lower components in stretched and jack-knifed states and can be traced back to the Schrödinger-like equations (20)–(21). This is in contrast to the amplitudes of the positive energy projections ($\tilde{\alpha}_\kappa$) that in all cases are strongly dominated by the upper component (g_κ) and are therefore similar for stretched and jack-knifed states. Note that $g_\kappa(r)$ for stretched and jack-knifed states (with equal n and ℓ) differ only in their *r.m.s.* radii.

Since the non-relativistic limit corresponds to $\tilde{\beta}_\kappa(p) = 0$, as a corollary we may also conclude that comparing to the non-relativistic limit, the responses for the stretched states will be closer than those for the jack-knifed states to their respective non-relativistic limits.

The choice of current operator and gauge is an important issue in quasielastic electron scattering since theoretical results on differential cross-sections and response functions depend substantially on those choices (see for instance refs. [13, 23, 24] and refs. therein). This tends to be particularly so when relativistic bound and/or scattering wave functions are used because the contributions from the negative energy projections depend more strongly on the current operator choice than do the contributions from the positive energy projections. The relativistic approach provides a tool to study further reaching consequences of the various choices of the current operators and gauges that can not be explored if one attaches to the non-relativistic description of the nuclear structure and wave functions where one can not go beyond the truncated expression in eq. (43).

In the case of stretched states the differences in the R^{TL} responses with different current operators and gauges are of the same order (and have the same origin) as those found with non-relativistic bound nucleon wave functions. The theoretical uncertainty for these states is at most a 20% (this is the largest ratio between CC1(3) and CC2(0) calculations), which is small compared to the large theoretical uncertainty of up to 300% found for the jack-knifed states. Although our calculations here do not contain final-state interactions, a similar behaviour is to be expected when FSI are included. Since FSI and short-range initial-state correlations are expected to play a similar role when calculating the R^{TL} response of different spin-orbit partners, the effect found here may provide a way to test different choices of current operators and gauges.

Since the results for jack-knifed states amplify differences between models, while those for the stretched states are more “model independent”, the combined analysis of data on spin-orbit partners can be used to elucidate between models. On the other hand, if one wants to determine with minimal model dependence a certain observable, one should focus on measurements on stretched states.

Acknowledgements

This work is supported in part by a NATO Collaborative Research Grant Number 940183, in part by DGICYT (Spain) under Contract Nos. PB/95-0123 and PB/95-0533-A, in part by Complutense University (Madrid) under Project No. PR156/97 and in part by funds provided by the US Department of Energy (D.O.E.) under cooperative agreement #DE-FC01-94ER40818.

References

- [1] J.A. Caballero, T.W. Donnelly, E. Moya de Guerra and J.M. Udías, *Nucl. Phys. A*632 (1998) 323.
- [2] I. Bobeldijk et al., *Phys. Rev. Lett* 73 (1994) 2684; J. Wesseling et al., *Phys. Rev. C*55 (1997) 2773; L. Lapikás, *Nucl. Phys. A*553 (1993) 297C.
- [3] J.M. Udías, P. Sarriguren, E. Moya de Guerra, E. Garrido and J.A. Caballero, *Phys. Rev. C*48 (1993) 2731.

- [4] J.M. Udías, P. Sarriguren, E. Moya de Guerra, E. Garrido and J.A. Caballero, *Phys. Rev. C* **51** (1995) 3246.
- [5] Y. Jin, D.S. Onley and L.E. Wright, *Phys. Rev. C* **45** (1992) 1311.
- [6] J.D. Walecka, *Ann. Phys. (N.Y.)* **83** (1974) 491.
- [7] B.D. Serot and J.D. Walecka, *Adv. Nucl. Phys.* **16** (1986) 1.
- [8] J.M. Udías, P. Sarriguren, E. Moya de Guerra and J.A. Caballero, *Phys. Rev. C* **53** (1996) R1488.
- [9] S. Gardner and J. Piekarewicz, *Phys. Rev. C* **50** (1994) 2822.
- [10] A. Picklesimer, J.W. Van Orden and S.J. Wallace, *Phys. Rev. C* **32** (1985) 1312; A. Picklesimer and J.W. Van Orden, *Phys. Rev. C* **35** (1987) 266; *C* **40** (1989) 290.
- [11] M. Hedayati-Poor, J.I. Johansson and H.S. Sherif, *Phys Rev C* **51** (1995) 2044.
- [12] T. de Forest, *Nucl. Phys. A* **392** (1983) 232.
- [13] H.W.L. Naus, S.J. Pollock, J.H. Koch and U. Oelfke, *Nucl. Phys. A* **509** (1990) 717; S. Pollock, H.W.L. Naus and J.H. Koch, *Phys. Rev. C* **53** (1996) 2304.
- [14] H.J. Bulten, Ph.D. Thesis, University of Utrecht (1992); L. Lapikás, *Nucl. Phys. A* **553** (1993) 297c; G.M. Spaltro et al., *Phys. Rev. C* **48** (1993) 2385.
- [15] L. Chinitz et al., *Phys. Rev. Lett.* **67** (1991) 568.
- [16] J.A. Caballero, T.W. Donnelly, E. Moya de Guerra and J.M. Udías, *work in progress*.
- [17] J.D. Bjorken and S.D. Drell, in *Relativistic Quantum Mechanics*, McGraw-Hill (1964).
- [18] C.J. Horowitz and B.D. Serot, *Nucl. Phys. A* **368** (1981) 503; *Phys. Lett. B* **86** (1979) 146.
- [19] C.J. Horowitz, D.P. Murdock, and B.D. Serot, in *Computational Nuclear Physics*, Springer-Verlag, Berlin, 1991.
- [20] E.J. Kim, *Phys. Lett. B* **174** (1986) 233; A.O. Gattone and J.P. Vary, *Phys. Lett. B* **219** (1989) 22.
- [21] J.N. Ginocchio, *Phys. Rev. Lett.* **78**, (1997) 436; J.N. Ginocchio and D.G. Madland, *Phys. Rev. C* **57** (1998) 1167.
- [22] C.M. Lederer and V.S. Shirley (Eds.), in *Table of isotopes*, John Wiley and Sons, New York (1978).
- [23] S. Boffi, C. Giusti and F. D. Pacati, *Phys. Rep.* **226** (1993), 1; S. Frullani and J. Mougey, in *Advances in Nuclear Physics*, edited by J.W. Negele and E. W. Vogt, volume 14, Plenum Press, New York (1984).
- [24] J.A. Caballero, T.W. Donnelly and G.I. Poulis, *Nucl. Phys. A* **555** (1993) 709; J.A. Caballero, T.W. Donnelly, G.I. Poulis, E. Garrido and E. Moya de Guerra, *Nucl. Phys. A* **577** (1994) 528; E. Garrido, J.A. Caballero, E. Moya de Guerra, P. Sarriguren and J.M. Udías, *Nucl. Phys. A* **584** (1995) 256.

Figure captions

- Figure 1: Semi-sum (left panels) and semi-difference (right panels) of the baryonic and scalar densities. Results are shown for the spin-orbit partners: $1p_{1/2}$ (thick-dotted line), $1p_{3/2}$ (thin-dotted line), and $1d_{3/2}$ (thick-dashed), $1d_{5/2}$ (thin-dashed). For comparison we also present results for the shell $3s_{1/2}$ (solid line).
- Figure 2: Same as fig. 1 for the vector current density (eq. (26)).
- Figure 3: Amplitudes $|\tilde{\alpha}_\kappa(p)|$ (top panel) and $|\tilde{\beta}_\kappa(p)|$ (bottom panel) for the shells: $1p_{1/2}$, $1p_{3/2}$, $1d_{3/2}$ and $1d_{5/2}$. The labeling of the various curves is the same as in fig. 1.
- Figure 4: Interference longitudinal-transverse response function R^{TL} (in units of fm^3) for the shells: $1p_{1/2}$ (top panels) and $1p_{3/2}$ (bottom panels) in ^{16}O . Panels on the left hand side correspond to results for the CC1 current operator and the gauges: Landau (solid line), Coulomb (dotted) and Weyl (dashed). Right hand panels show the results for the CC2 current operator and the same labeling.
- Figure 5: Same as fig. 4 for the spin-orbit partners: $1d_{3/2}$ and $1d_{5/2}$.
- Figure 6: Components of the transverse-longitudinal response, R_P^{TL} , R_C^{TL} and R_N^{TL} (see eqs. (36–38)). Results are shown for the spin-orbit partners: $1p_{1/2}$ (top panel) and $1p_{3/2}$ (bottom panel). Thick lines correspond to gauges that use the CC2 current operator and thin lines correspond to the CC1 operator. Gauges considered are: Landau (solid lines), Coulomb (dotted lines) and Weyl (dashed lines).
- Figure 7: Same as fig. 6 for the shells: $1d_{3/2}$ (top panel) and $1d_{5/2}$ (lower panel).

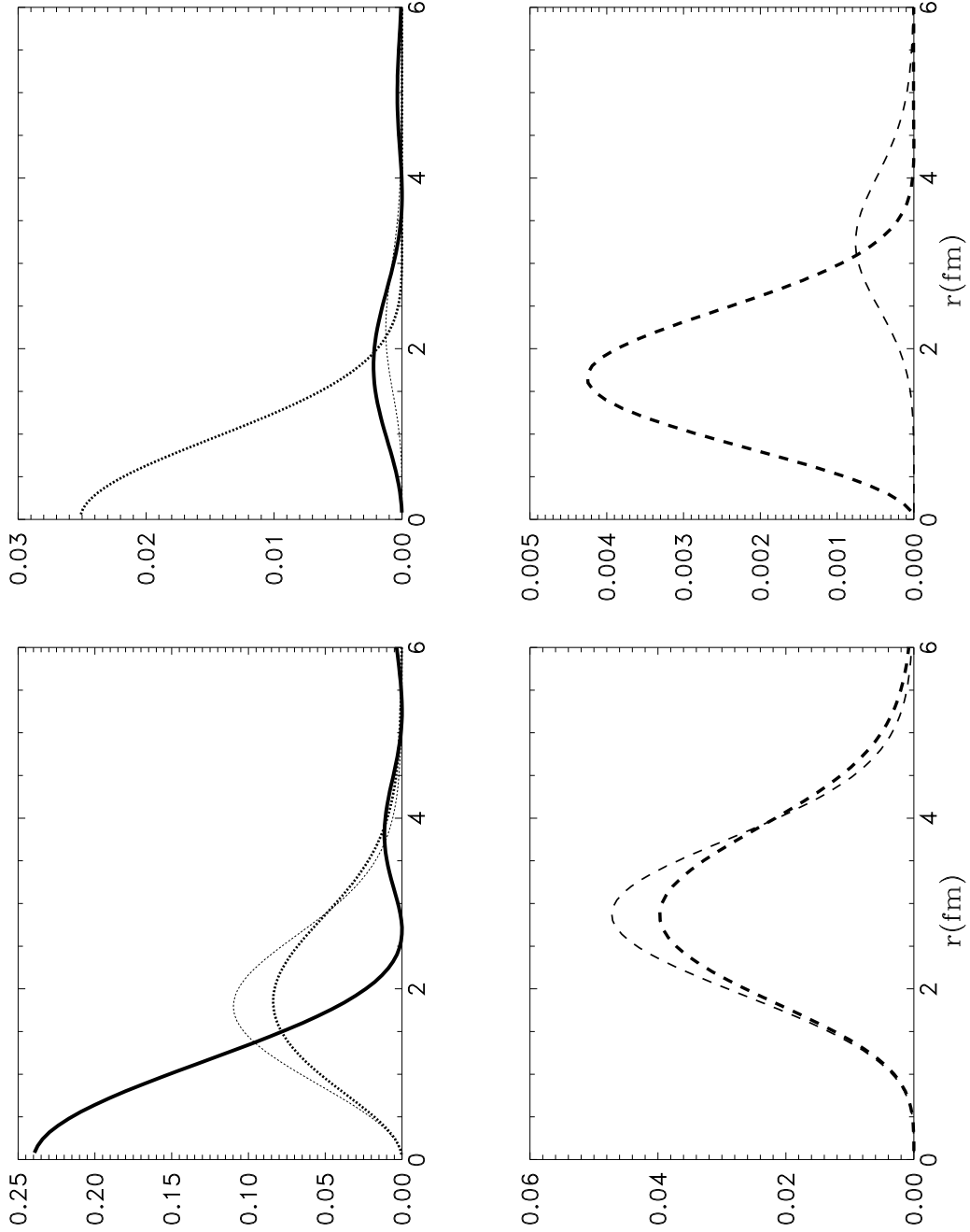


Figure 1: Semi-sum (left panels) and semi-difference (right panels) of the baryonic and scalar densities. Results are shown for the spin-orbit partners: $1p_{1/2}$ (thick-dotted line), $1p_{3/2}$ (thin-dotted line), and $1d_{3/2}$ (thick-dashed), $1d_{5/2}$ (thin-dashed). For comparison we also present results for the shell $3s_{1/2}$ (solid line).

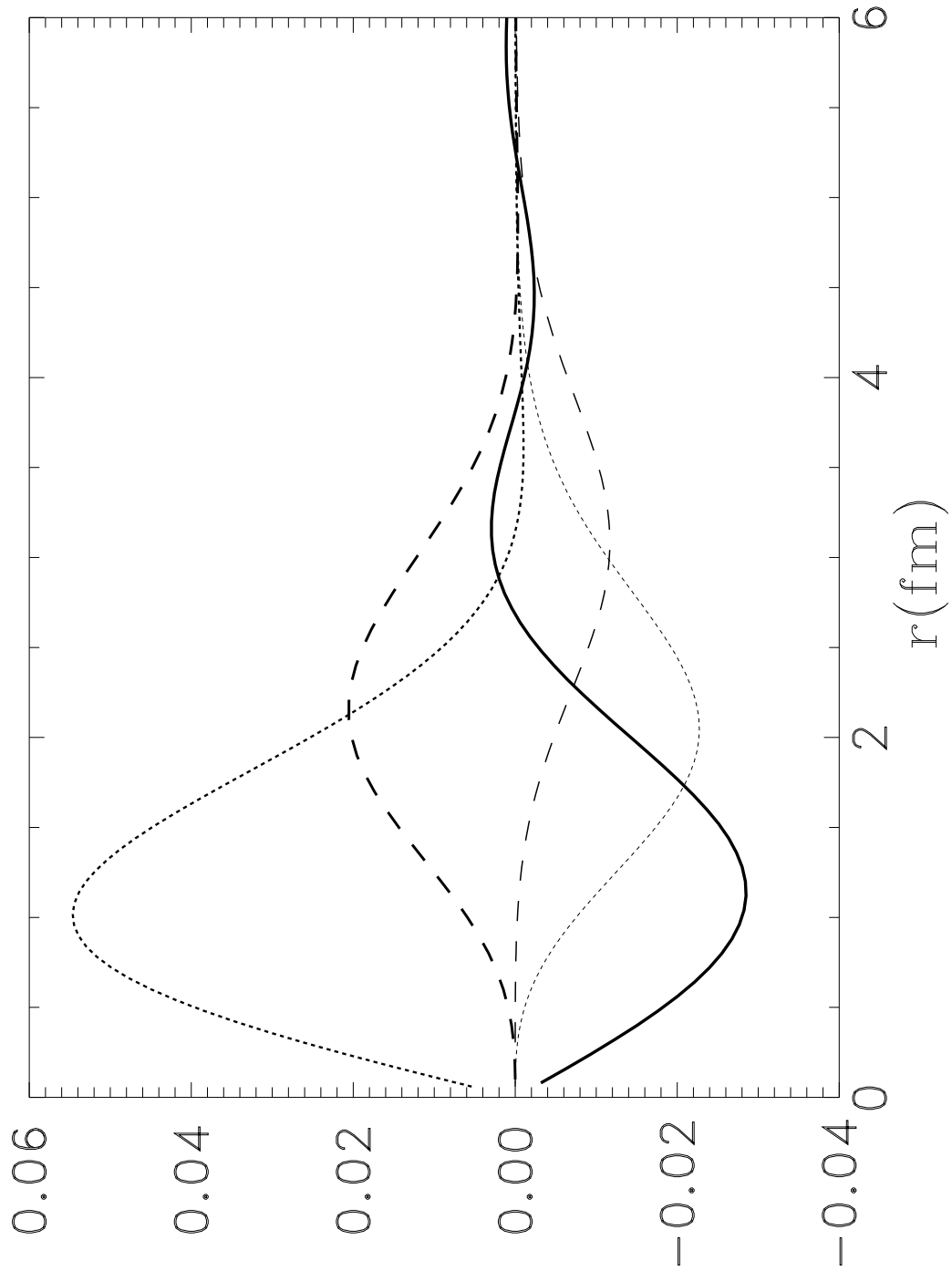


Figure 2: Same as fig. 1 for the vector current density (eq. (26)).

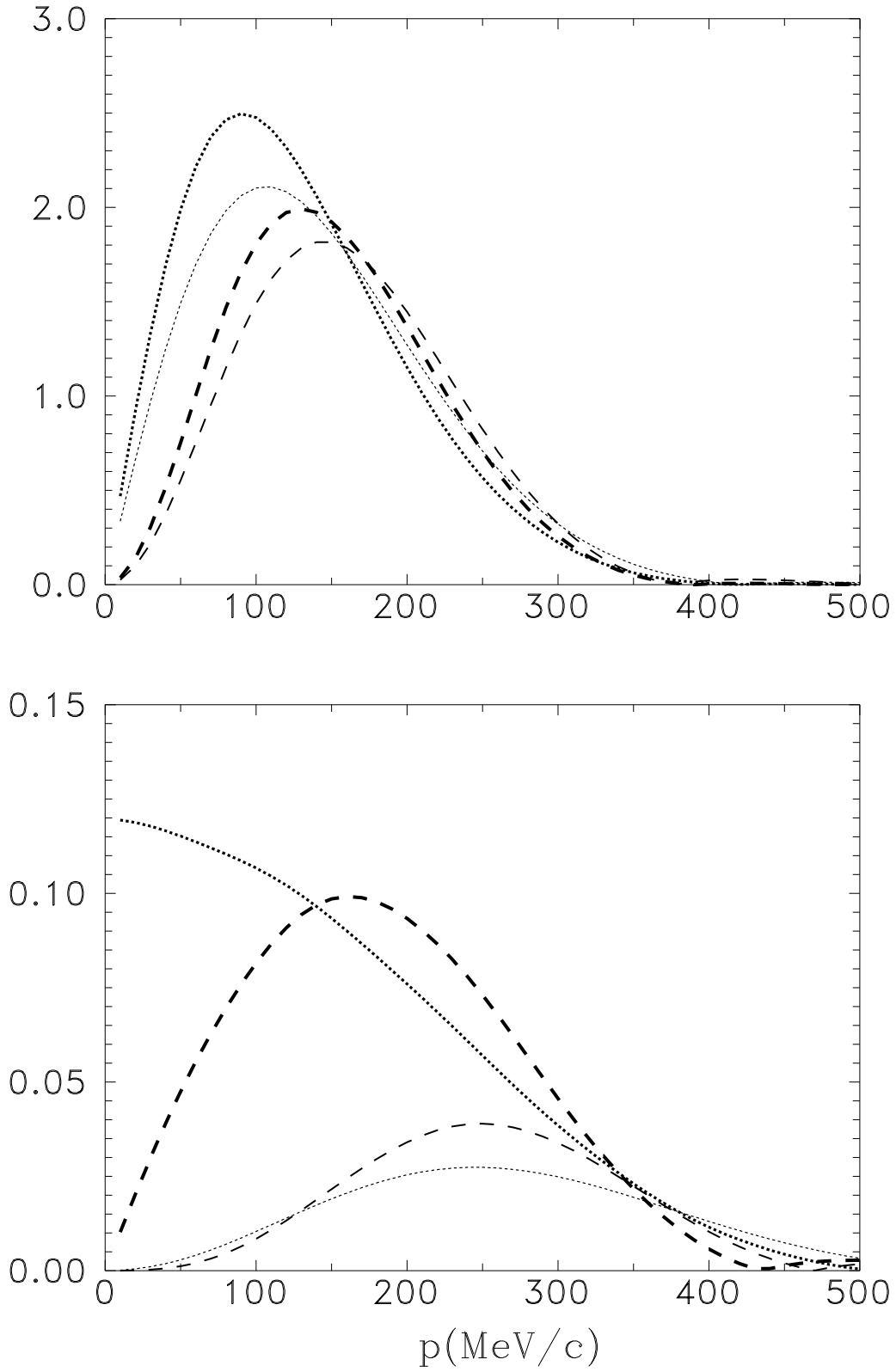


Figure 3: Amplitudes $|\tilde{\alpha}_\kappa(p)|$ (top panel) and $|\tilde{\beta}_\kappa(p)|$ (bottom panel) for the shells: $1p_{1/2}$, $1p_{3/2}$, $1d_{3/2}$ and $1d_{5/2}$. The labeling of the various curves is the same as in fig. 1.

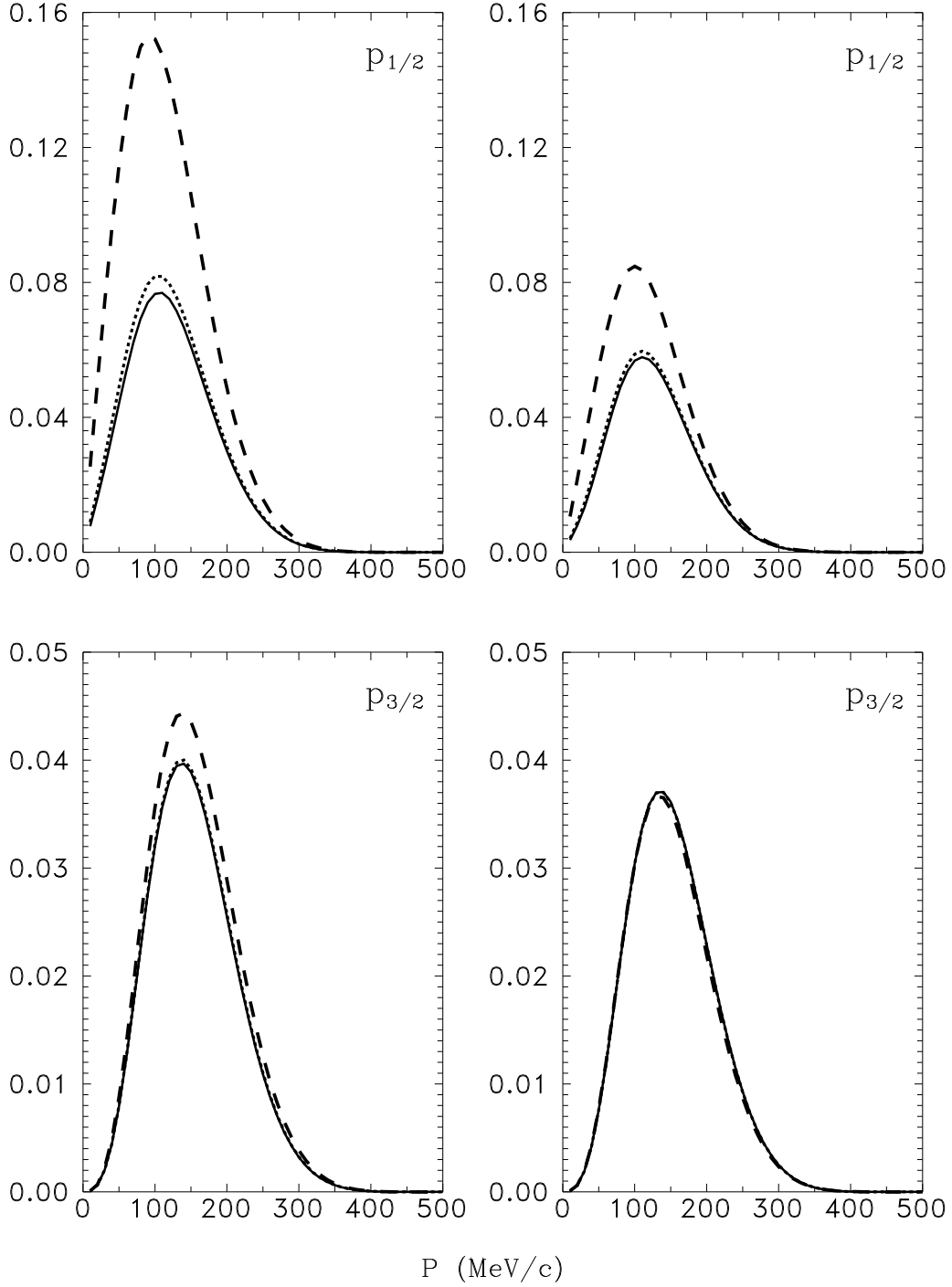


Figure 4: Interference longitudinal–transverse response function R^{TL} (in units of fm^3) for the shells $1p_{1/2}$ (top panels) and $1p_{3/2}$ (bottom panels) in ^{16}O . Panels on the left hand side correspond to results for the CC1 current operator and the gauges: Landau (solid line), Coulomb (dotted) and Weyl (dashed). Right hand panels show the results for the CC2 current operator and the same labeling.

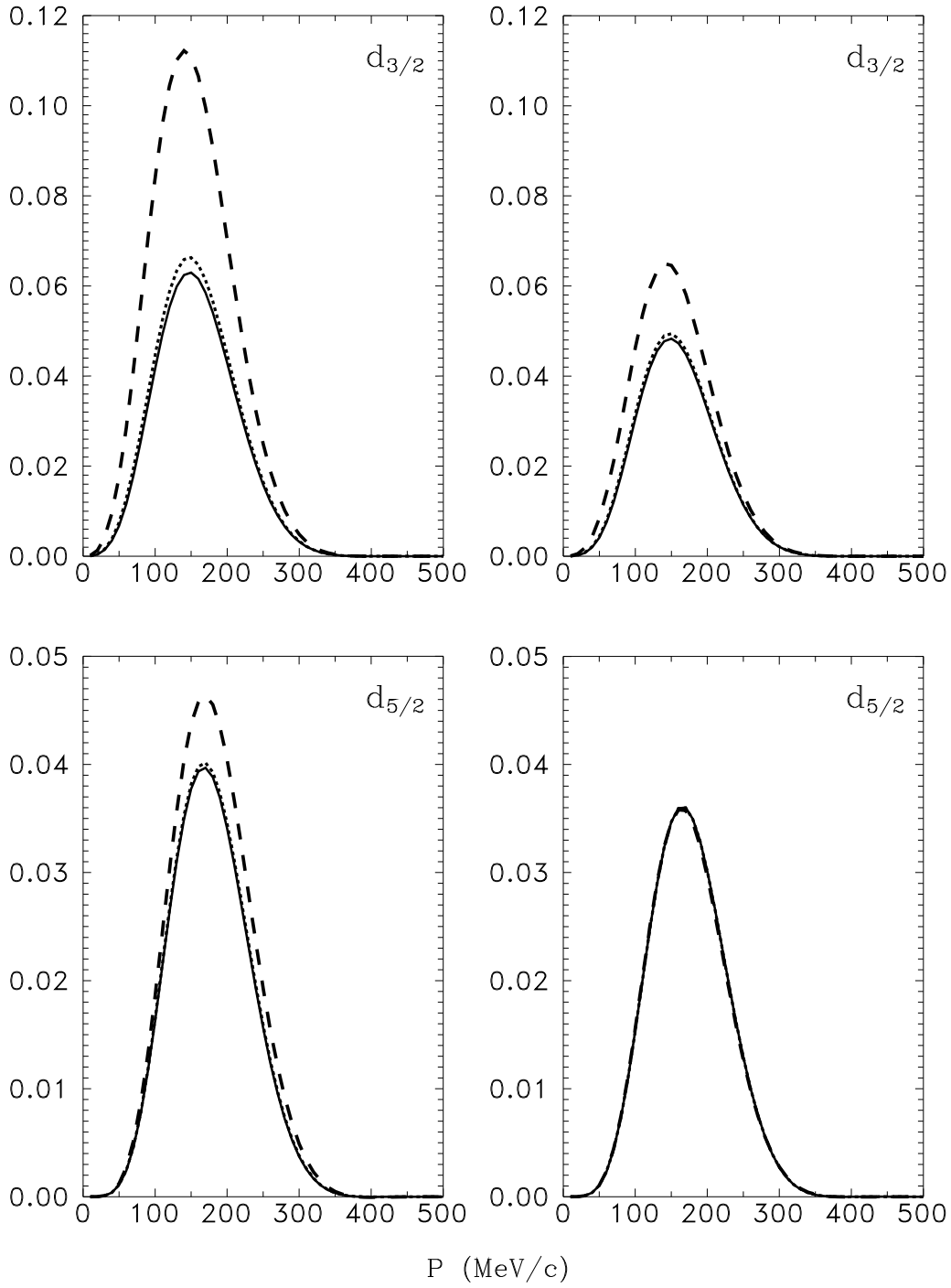


Figure 5: Same as fig. 4 for the spin-orbit partners: $1d_{3/2}$ and $1d_{5/2}$.

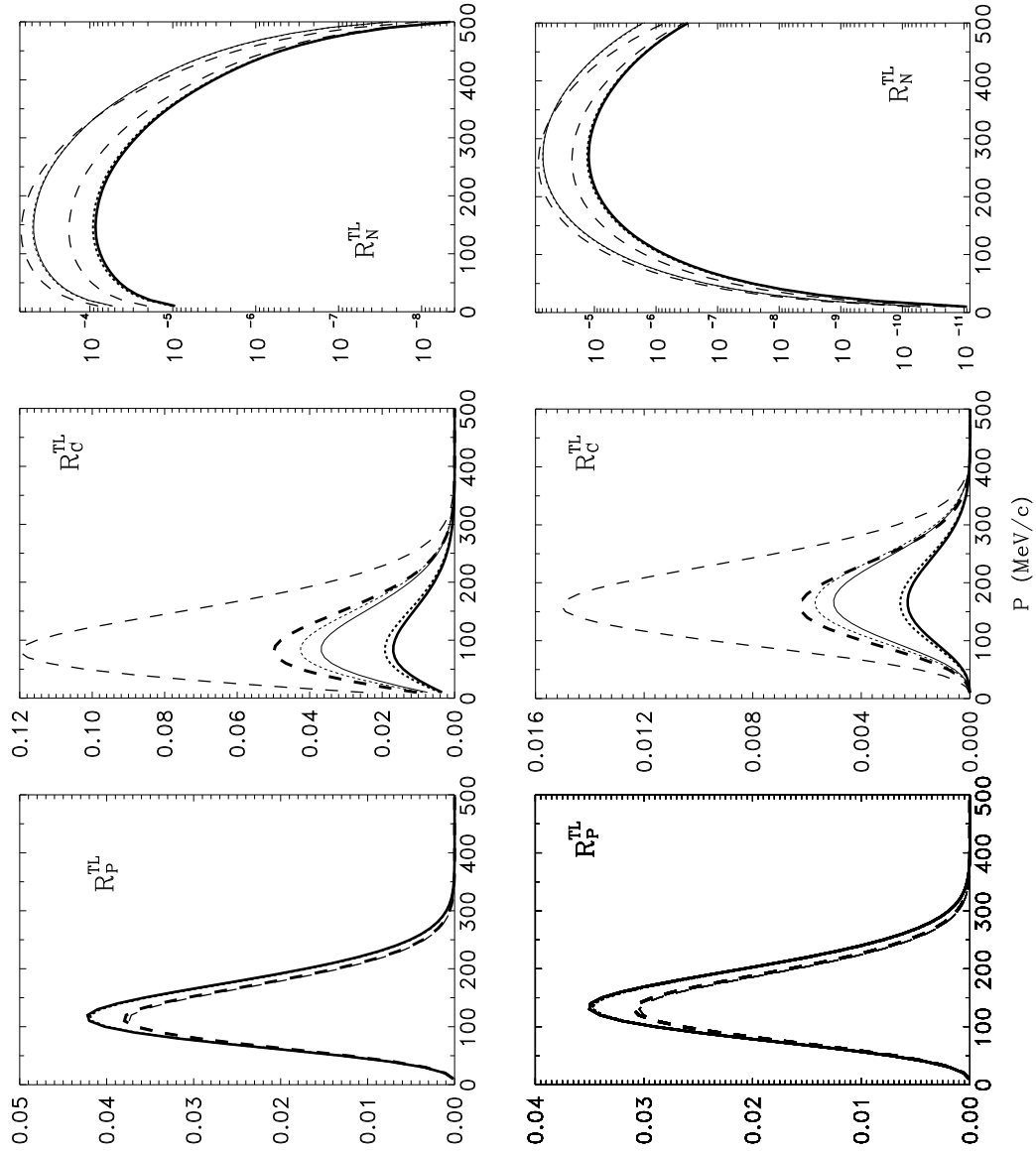


Figure 6: Components of the transverse-longitudinal response, R_P^{TL} , R_C^{TL} and R_N^{TL} (see eqs. (36-38)). Results are shown for the spin-orbit partners: $1p_{1/2}$ (top panel) and $1p_{3/2}$ (bottom panel). Thick lines correspond to gauges that use the CC2 current operator and thin lines correspond to the CC1 operator. Gauges considered are: Landau (solid lines), Coulomb (dotted lines) and Weyl (dashed lines).

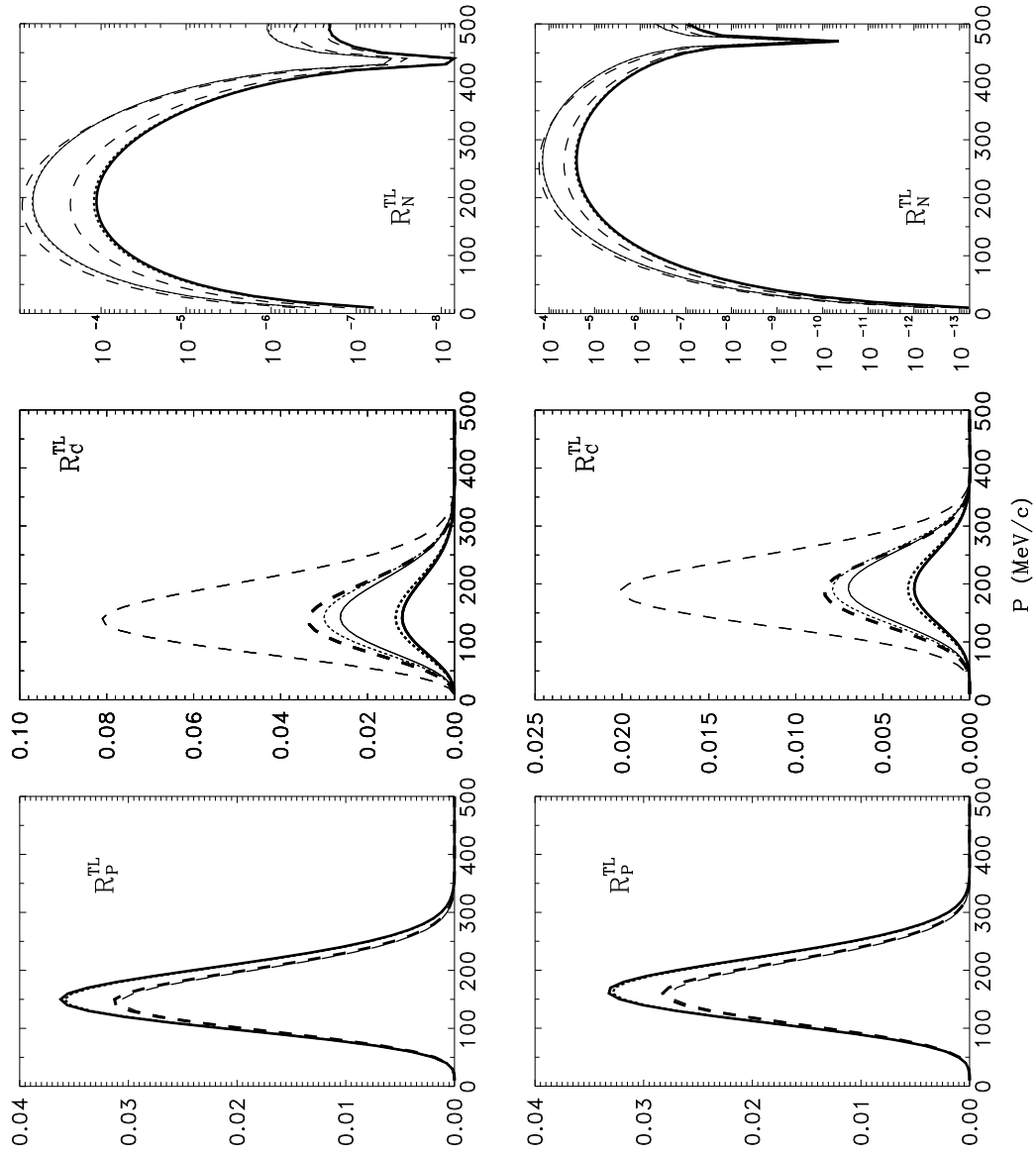


Figure 7: Same as fig. 6 for the shells: $1d_{3/2}$ (top panel) and $1d_{5/2}$ (lower panel).